

NASA TECHNICAL NOTE



NASA TN D-3469

NASA TN D-3469



EXPERIMENTAL AND THEORETICAL PERFORMANCE OF COAXIAL PLASMA GUNS

by Charles J. Michels and Albert E. Johansen

*Lewis Research Center
Cleveland, Ohio*



EXPERIMENTAL AND THEORETICAL PERFORMANCE
OF COAXIAL PLASMA GUNS

By Charles J. Michels and Albert E. Johansen

Lewis Research Center
Cleveland, Ohio

NATIONAL AERONAUTICS AND SPACE ADMINISTRATION

For sale by the Clearinghouse for Federal Scientific and Technical Information
Springfield, Virginia 22151 - Price \$2.00

EXPERIMENTAL AND THEORETICAL PERFORMANCE OF COAXIAL PLASMA GUNS^{*}

by Charles J. Michels and Albert E. Johansen

Lewis Research Center

SUMMARY

Experimentally determined calorimetric exhaust efficiencies and exhaust velocities are compared with predicted values from a snowplow model analysis. Four gun geometries (employing argon propellant) are examined analytically and experimentally over a range of initial masses and voltages. Noncrowbarred and crowbarred results are described. Experimentally stable operation of a gun has been limited to mass distributions for which a simplified analysis limits maximum efficiencies to about 40 percent. Experimentally measured efficiencies for optimum propellant distributions are approximately one-half those predicted from the simplified analysis (the maximum experimental efficiency was 22.2 percent). Experimental efficiencies agree somewhat better with peak efficiencies predicted by the complete theory. Experimental velocities agree approximately with both forms of the theory, but are generally somewhat lower.

INTRODUCTION

During 1964-65, experiments with coaxial plasma guns (all powered by conventional capacitor banks) were conducted at the Lewis Research Center. Measurements of kinetic efficiency based on calorimetric techniques and of magnetic front velocity of the plasma sheet in the gun were made for several gun geometries with wide ranges of injected mass and initial bank voltage.

In order to interpret the experimental results, correlate the data, and determine the parameters important for efficient gun design, a theoretical model was developed and analyzed. The initial description of the theory for this model is given in reference 1.

^{*}Part of this report incorporates, in condensed fashion, portions of a paper presented at the Second Annual Meeting of the AIAA, given at San Francisco, California on July 26, 1965 (ref. 1).

Like many previous theories (refs. 2 to 5), it is based on the so-called snowplow model of mass sweep-up by the current sheet but allows for a variable initial mass distribution and includes, as a special case, the slug model (refs. 6 to 9).¹ For convenience, the mass distributions used to calculate the theoretical results presented herein are limited to members of a one-parameter family ranging from a constant distribution to that of a slug. In addition to variable initial mass distribution, this analysis includes the effect of losses associated with wall drag due to ion thermal diffusion, electron heat conduction, ohmic losses, ionization, and radiation. The assumed model leads to three coupled differential equations: one for the charge on the capacitor (Kirchoff's law), one for the displacement of the discharge (the momentum equation), and one for the plasma temperature (the plasma energy equation). The equations were integrated numerically with a high-speed digital computer.

Theoretical results for various gun geometries are given for a simplified version of the analysis and also for the case in which all the mentioned losses are included. The simplified version includes only ohmic and shock heating losses. These results are presented for comparison with the experimental data for both the noncrowbarred and crowbarred modes of gun operation.

The experimental data allow only limited comparison with the theory. The total injected mass and the initial bank voltages were varied in a systematic way for each gun geometry investigated, while the other quantities were held constant. Some argon data previously reported by Michels and Ramins (ref. 15) have been included. The magnetic front velocities are measured in each gun annulus. No attempt is made to describe the plasma structure after it leaves the gun muzzle. This structure depends on the mode of operation of the gun and is described for a particular case by Michels (ref. 16). Ion velocity distributions in the exhaust, as described for particular cases in references 17 to 20, were not examined in this work.

An external crowbar system is described in appendix B by Fred F. Terdan.

The meter-kilogram-second system of units is used throughout and the symbols are defined in appendix A.

THEORY

Three coupled nonlinear differential equations describe the capacitor-driven plasma gun system. The first two equations, the circuit and the momentum equations, involve functions of plasma temperature. The third equation is the plasma energy equation,

¹Other models that have been analytically treated include the gas dynamic model (refs. 10 to 12) and the elastic piston model (ref. 13). The snowplow model has been justified to a limited extent by Hart (ref. 5) and Mather (ref. 14).

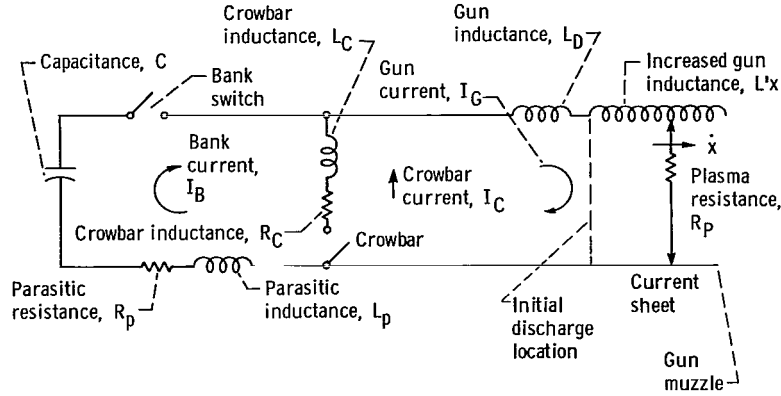


Figure 1. - Equivalent gun circuit.

which is necessary to determine plasma temperature. The derivation of the theory presented in reference 1 is reviewed in the following sections.

Circuit Equations

The equivalent gun circuit is shown in figure 1. Before crowbar occurs, I_C is zero, and $I_B = I_G = I$. Kirchoff's equation for a circuit may be obtained by deriving an energy equation for the circuit, differentiating it with respect to time, and dividing it by the current. This approach is used in this analysis to account conveniently for the electrical energy losses associated with ionization and excitation of the plasma. The fraction of the ionization and excitation that is not produced directly by electrical energy is considered to be accomplished at the expense of plasma thermal energy. This fraction, denoted by $P(T)$, is a function of the plasma temperature. It is assumed that the plasma is always 100 percent ionized and a constant fraction g (assumed unity herein) of the ions are in an excited state corresponding to some single effective quantum level estimated from spectroscopic observations and knowledge of excited states.

With these assumptions, the electrical energy absorbed in ionizing and exciting particles that are swept up by the discharge current sheet and in reionizing and reexciting particles that have diffused to the walls may be written as

$$\int_0^t \Phi_1 [1 - P(T)] \left[\frac{d}{dt} \left(\frac{M}{m_i} \right) + \Gamma(T) \right] dt$$

where $\Phi_1 = \Phi_i + g\Phi_e$, M is the mass swept up by the current sheet, m_i is the ion mass,

and $\Gamma(T)$ is the diffusion rate of ions to the walls. The symbols Φ_i and Φ_e are, in turn, defined as the effective ionization and excitation potentials. The electrical energy lost by radiation (i. e., by maintaining the excitation of ions in the discharge) may be written as

$$\int_0^t \Phi_2 \left[1 - P(T) \right] \left(\frac{M}{m_i} \right) dt$$

where $\Phi_2 = g(\Phi_e/t_e)$ is the excitation loss rate parameter and t_e is the mean lifetime of the excited state.

The remaining terms in the energy equation for the circuit are familiar and should require no explanation. The complete circuit energy equation is

$$\begin{aligned} \frac{1}{2} CV_0^2 = \frac{1}{2} CV^2 + \frac{1}{2} (L_p + L_D + L'_x) I^2 + \int_0^t (R_p + R_P) I^2 dt \\ + \int_0^t F_x \frac{dx}{dt} dt + \int_0^t \left[1 - P(T) \right] \left\{ \Phi_1 \left[\frac{d}{dt} \left(\frac{M}{m_i} \right) + \Gamma(T) \right] + \left(\frac{M}{m_i} \right) \Phi_2 \right\} dt \end{aligned} \quad (1)$$

where

$$F_x = \frac{1}{2} L' I^2$$

is the x-component of the Lorentz force integrated over the discharge volume. Differentiation of the energy equation and subsequent division by I (where $I = -C(dV/dt)$) produces the following circuit equation:

$$\begin{aligned} -V + (L_p + L_D + L'_x) \frac{dI}{dt} + \frac{1}{2} L' \frac{dx}{dt} I + (R_p + R_P) I \\ + \frac{1}{2} L' \frac{dx}{dt} I + \frac{1}{I} \left[1 - P(T) \right] \left\{ \Phi_1 \left[\frac{d}{dt} \left(\frac{M}{m_i} \right) + \Gamma(T) \right] + \left(\frac{M}{m_i} \right) \Phi_2 \right\} = 0 \end{aligned} \quad (2)$$

The terms in this equation correspond, respectively, to the following voltage drops: condenser (negative), inductance, increase in new magnetic field volume, resistance,

work done on the discharge, and finally, ionization and excitation (radiation). Note that the third and fifth terms are identical; that is, the voltage drop associated with the increase in magnetic field is the same as the voltage drop associated with the mechanical work done on the plasma. When the terms are collected, the circuit equation may be written as

$$V = (R_p + R_p)I + \frac{d}{dt} [(L_p + L_D + L'x)I] + \frac{1}{I} [1 - P(T)] \left\{ \Phi_1 \left[\frac{d}{dt} \left(\frac{M}{m_i} \right) + \Gamma(T) \right] + \left(\frac{M}{m_i} \right) \Phi_2 \right\} \quad (3)$$

Equation (3) has been derived for a single moving discharge. In typical gun operation, a secondary discharge occurs which may be either moving or stationary. If stationary, it is called a crowbar discharge. The resulting circuit diagram is also illustrated in figure 1. Equation (3) is used prior to the time when crowbar occurs. When crowbar occurs, the crowbar "switch" may be assumed to close, and the following equations describe the resulting circuit:

$$V = R_p I_B + R_p I_G + \frac{d}{dt} (L_p I_B + L_D I_G + L'x I_G) + \frac{1}{I_G} [1 - P(T)] \left\{ \Phi_1 \left[\frac{d}{dt} \left(\frac{M}{m_i} \right) + \Gamma(T) \right] + \left(\frac{M}{m_i} \right) \Phi_2 \right\} \quad (3a)$$

$$0 = R_p I_G + R_C I_C + \frac{d}{dt} (L_D I_G + L_C I_C + L'x I_G) + \frac{1}{I_G} [1 - P(T)] \left\{ \Phi_1 \left[\frac{d}{dt} \left(\frac{M}{m_i} \right) + \Gamma(T) \right] + \left(\frac{M}{m_i} \right) \Phi_2 \right\} \quad (3b)$$

Momentum Equation

The snowplow model assumes that the discharge current sheet sweeps up the mass it encounters and carries it at sheet velocity. In addition, all the directed momentum of a particle striking the gun walls is assumed to be lost to the wall. The momentum equation is therefore

$$\frac{d}{dt} \left(M \frac{dx}{dt} \right) = \frac{1}{2} L' I_G^2 - m_i \Gamma(T) \frac{dx}{dt} \quad (4)$$

which merely states that the time rate of change of plasma momentum is equal to the force on the discharge minus the momentum lost to the walls by ion thermal diffusion.

Plasma Energy Equation

The plasma energy equation is written for a frame of reference moving with the current sheet and is used to determine the static plasma temperature T that is required to evaluate Γ . In this frame of reference, each particle entering the discharge (either initially or following contact with a wall) appears to be moving with a velocity $-dx/dt$ and possesses a kinetic energy $1/2 m_i (dx/dt)^2$. The plasma energy equation states that the rate of thermal energy increase can be equated to the algebraic sum of the rate of heating due to thermalization of the kinetic energy of particles entering the discharge and the rate of cooling due to various assumed loss mechanisms. It can be written as

$$\begin{aligned} \frac{d}{dt} \left[\frac{3}{2} kT(1+z) \left(\frac{M}{m_i} \right) \right] = R_P I_G^2 + \frac{1}{2} \frac{dM}{dt} \left(\frac{dx}{dt} \right)^2 + \frac{1}{2} m_i \Gamma(T) \left(\frac{dx}{dt} \right)^2 - \frac{3}{2} kT(1+z) \Gamma(T) \\ - P(T) \left\{ \Phi_1 \left[\frac{d}{dt} \left(\frac{M}{m_i} \right) + \Gamma(T) \right] + \left(\frac{M}{m_i} \right) \Phi_2 \right\} - \int_{\text{wall}} (-K \nabla T) dS - \frac{3}{2} kT \frac{|I_G|}{e} \end{aligned} \quad (5)$$

where the terms on the right side of the equation are respectively due to, ohmic heating, thermalization of the kinetic energy of the swept-up mass, rethermalization of the particles rebounding from the walls, convective losses associated with particle diffusion, ionization and radiation losses, conductive losses of heat in the electron gas, and convective losses associated with the main electron conduction current. Wall drag effects are taken into account in the last term of equation (4) and the fourth term on the right side of equation (5). Approximate expressions for $\Gamma(T)$, $\int_{\text{wall}} (-K \nabla T) dS$, and K used throughout this report are

$$\Gamma(T) = \frac{1}{2} \left(\frac{M}{m_i} \right) \frac{1}{(r_o - r_i)} \sqrt{\frac{2kT}{m_i}}$$

$$\int_{\text{wall}} (-K \nabla T) dS = 7.77 \pi K \Delta x \left(\frac{r_o + r_i}{r_o - r_i} \right) T$$

and

$$K = \frac{75}{32 \sqrt{\pi}} \left[\sqrt{m_e} \left(\frac{e^2}{4\pi\epsilon_0} \right)^2 \ln \Lambda \right]^{-1} k(kT)^{5/2}$$

The expression for Γ is just one-fourth of the product of the thermal velocity, number density, and area, correct for an isotropic velocity distribution. The rate of heat loss by conduction in the electron gas was deduced from an analysis of a simplified situation, namely, steady-state conduction between isothermal slabs with uniform heat source density. The thermal conductivity of the electron gas K is as described in reference 21.

Nondimensional Equations

The three nonlinear coupled differential equations (eqs. (3), (4), and (5)) completely describe the system consisting of capacitor, gun, and plasma. The fraction $P(T)$ must also be specified and was assumed zero for all the calculations. In order to generalize the equations and facilitate their solution, the following nondimensional variables and parameters are introduced:

$$\left. \begin{aligned} \tau &= (L'\ell C)^{-1/2} t; \quad \mathcal{L} = \left(\frac{1}{L'\ell} \right) L; \quad \xi = \ell^{-1} x; \quad f = \frac{M(x)}{M_0}; \quad \gamma = Q_0^{-1} Q \\ \beta &= \frac{2k}{m_i} \left(\frac{L'C}{\ell} \right) T; \quad \mathcal{M} = \left(\frac{2\ell}{L'Q_0^2} \right) M_0; \quad \delta = \left[\frac{1}{2(r_0 - r_i)} \right] \ell; \quad \mathcal{R} = \sqrt{\frac{C}{L'\ell}} R \\ \varphi_1 &= \left(\frac{L'C}{m_i\ell} \right) (\Phi_i + g\Phi_e); \quad \varphi_2 = \left(\frac{L'C}{m_i\ell} \right) \frac{\sqrt{L'C\ell}}{t_e} g\Phi_e; \quad \Omega = \frac{3}{2} \frac{\frac{m_i\ell}{L'C}}{eV_0} \\ \mathcal{J} &= 2.85 \left(\frac{r_0 + r_i}{r_0 - r_i} \right) \left(\frac{\Delta x}{\ell} \right) \sqrt{\frac{m_i}{m_e}} \left(\frac{\frac{m_i\ell}{L'C}}{\frac{1}{2} CV_0^2} \right) \frac{\ell^2 \left(\frac{m_i\ell}{L'C} \right)^2}{\left(\frac{e^2}{4\pi\epsilon_0} \right)^2 \ln \Lambda} \end{aligned} \right\} \quad (6)$$

A mass density distribution in the x-direction $M_0(df/dx)$ was so chosen that a family of distributions could be represented from a "slug" to a constant density profile. The function

$$f = 1 - (1 - \xi)^{1/(1-\alpha)} \quad (7)$$

was used in which α varies from zero (constant density) to 1 (slug).

Before crowbar occurs, the nondimensional system equations can be written as follows:

Circuit equation:

$$\gamma + (\mathcal{L}_p + \mathcal{L}_D)\ddot{\gamma} + (\mathcal{R}_p + \mathcal{R}_D)\dot{\gamma} + \xi\dot{\gamma} + \xi\ddot{\gamma} + \frac{1}{2}\mathcal{M}\left(\frac{1}{\dot{\gamma}}\right) \left[\varphi_1(f'\xi + \delta f\beta^{1/2}) + \varphi_2 f \right] = 0 \quad (8)$$

Momentum equation:

$$\mathcal{M}f\xi^2 + \mathcal{M}f\xi\ddot{\xi} = \dot{\gamma}^2 - \delta\mathcal{M}f\xi\beta^{1/2} \quad (9)$$

Plasma energy equation:

$$\frac{3}{4}(1+z)\mathcal{M}(f'\xi\beta + f\dot{\beta}) = 2\mathcal{R}_p\dot{\gamma}^2 + \frac{1}{2}\mathcal{M}(f'\xi + \delta f\beta^{1/2})\xi^2 - \frac{3}{4}(1+z)\delta\mathcal{M}f\beta^{3/2} - \mathcal{J}\beta^{7/2} - \Omega|\dot{\gamma}|\beta \quad (10)$$

Not an explicit part of the system of equations but available from the calculations are the kinetic efficiency η

$$\eta \equiv \left[\frac{\frac{1}{2} M \left(\frac{dx}{dt} \right)^2}{\frac{1}{2} CV_0^2} \right]_{x=\ell} = \left(\frac{1}{2} \mathcal{M} f \xi^2 \right)_{\xi=1}$$

and the nondimensional velocity $\dot{\xi}$

$$\dot{\xi} \equiv \left(\frac{d\xi}{d\tau} \right)_{\xi=1} = \frac{\sqrt{L'C}}{\sqrt{\ell}} \left(\frac{dx}{dt} \right)_{x=\ell}$$

After crowbar occurs, there is a similar set of nondimensional equations that are complicated as a result of the extra circuit involved. These are written as follows:

Circuit equations:

$$\gamma + \mathcal{L}_P \ddot{\gamma} + \mathcal{R}_B \dot{\gamma} - \mathcal{L}_D \dot{\mathcal{J}} - (\dot{\xi} \mathcal{J} + \xi \dot{\mathcal{J}}) - R_P \mathcal{J} - \mathcal{J}^{-1} \left\{ \frac{1}{2} \mathcal{M} \left[\varphi_1 (f' \dot{\xi} + \delta f \beta^{1/2}) + \varphi_2 f \right] \right\} = 0 \quad (11)$$

$$(\dot{\xi} \mathcal{J} + \xi \dot{\mathcal{J}}) + (\mathcal{L}_D + \mathcal{L}_C) \dot{\mathcal{J}} + R_P \mathcal{J} + R_C \mathcal{J} + \mathcal{L}_C \ddot{\gamma} + R_C \dot{\gamma} + \frac{1}{2} \mathcal{M} \mathcal{J}^{-1} \left[\varphi_1 (f' \dot{\xi} + \delta f \beta^{1/2}) + \varphi_2 f \right] = 0 \quad (12)$$

Momentum equation:

$$\mathcal{M} f' \dot{\xi}^2 + \mathcal{M} f \ddot{\xi} = (-\mathcal{J})^2 - \delta \mathcal{M} f \dot{\xi} \beta^{1/2} \quad (13)$$

Plasma energy equation:

$$\begin{aligned} \frac{3}{4} (1 + z) \mathcal{M} (f' \dot{\xi} \beta + f \dot{\beta}) &= 2 R_P (-\mathcal{J})^2 + \frac{1}{2} \mathcal{M} (f' \dot{\xi} + \delta f \beta^{1/2}) \dot{\xi}^2 \\ &\quad - \frac{3}{4} (1 + z) \delta \mathcal{M} f \beta^{3/2} - \mathcal{J} \beta^{7/2} - \Omega |(-\mathcal{J})| \beta \end{aligned} \quad (14)$$

In equations (11), (12), (13), and (14), the additional complication of crowbar circuitry requires that extra nondimensional current variables be defined, namely,

$$\begin{aligned} \dot{\gamma} &= \frac{I_B}{C V_0 / (L' l C)^{1/2}} \\ \mathcal{J} &= \frac{I_G}{C V_0 / (L' l C)^{1/2}} \end{aligned}$$

Theoretical Performance

The nondimensional system equations were solved by numerical techniques for two

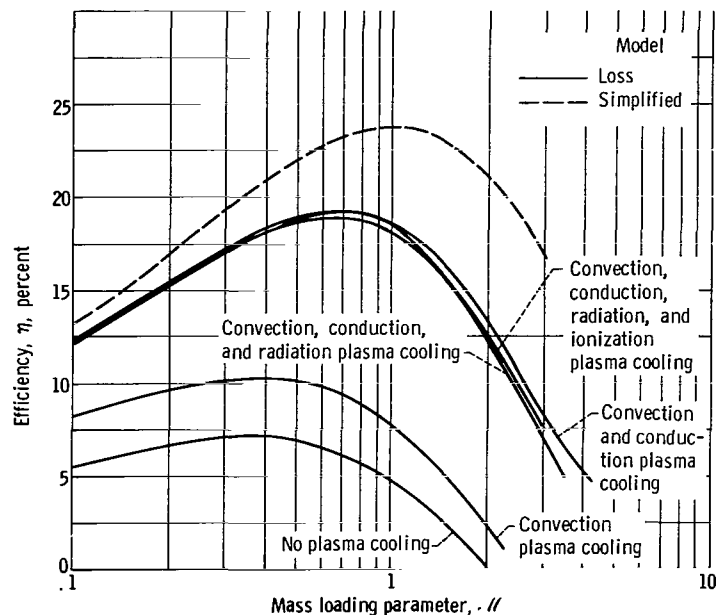


Figure 2. - Effect of plasma cooling on kinetic efficiency for geometry A. Non-crowbarred; nondimensional mass distribution parameter, $1/2$.

different cases, a simplified model and a loss model. Ohmic losses and losses due to shock heating are included in the simplified model. The loss model includes the plasma cooling terms accounted for in equations (8), (9), and (10). The effect of these cooling terms on efficiency is shown in figure 2 for a particular case (noncrowbarred, $\alpha = 1/2$, geometry A, described on p. 20). The effect of wall drag on efficiency is dominant. If no plasma cooling mechanisms are considered, the resulting high temperatures of the plasma sheet enhance the diffusion to the walls, and the loss of momentum to the walls limits the maximum efficiency to 7.1 percent. Some cooling of the plasma is necessary to increase the efficiency to near observed values, which generally are above the values shown by the lower curves of figure 2. Although such cooling is also an energy loss, it is not a momentum loss. In fact, it reduces the drag loss so that the overall effect is an increase in kinetic efficiency. Results for other configurations are presented in the section COMPARISON OF THEORY WITH EXPERIMENT along with the corresponding experimental data.

The useful thrust of the device is the sum of the rate of momentum flux through the exit plane and the force equal to the product of exit pressure and exit area. The theoretical calculation of efficiency has not taken into account the pressure effect. In the simplified model, sample calculations incorporating the pressure term have shown that theoretical efficiencies increase a few percent. In the loss model, however, the plasma cooling has reduced the sheet pressure so that the effect is negligible.

In reference 1 it is shown that the simplified model efficiencies were greatest for the

slug mass distribution, for M near 1, and \mathcal{L}_{tot} near 0.1. Also, crowbarring (at either maximum current time or maximum energy time, that is, the time when the useful energy available for plasma acceleration after crowbar is a maximum) does not give a higher maximum efficiency than the corresponding noncrowbar case. Crowbarring at the time of maximum available energy was found to have higher efficiency for M greater than 1.0 than either of the other two modes of operation. If for other reasons, such as stability or breakdown delay time, a gun were operated at M greater than 1.0, crowbarring at maximum energy would give the highest efficiency, other factors being held constant.

Crowbarred loss model cases are not included in reference 1, but they have since been calculated, and the results are presented herein. Generally, the incorporation of losses in the crowbarred analysis shows that efficiencies at values above M equal to 1.5 are less than the corresponding noncrowbarred case. Previously, crowbarring was considered advantageous for M greater than 1.0 (ref. 1). This advantage, however, is more than negated by the fact that losses are severe for M greater than 1.0.

APPARATUS

Capacitor Bank

The guns described in this report were energized by a capacitor bank consisting of 11 identical sections switched simultaneously through cabling to the coaxial plasma gun. Each section consists of a 1.1-microfarad capacitor, a GL-7703 ignitron switch, and three parallel coaxial cables. The 5000-Joule bank, which has a resistance of 3.3 milliohms and an inductance of 14 nanohenries, is discussed in detail in reference 22.

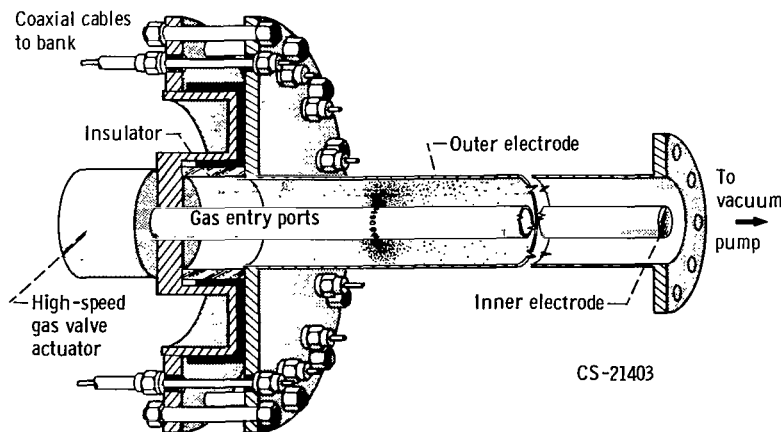


Figure 3. - Coaxial plasma gun.

Gun Geometries

Figure 3 shows the coaxial gun and the manner in which it is connected to the bank cables. The electrodes of each of the guns are made of oxygen-free high-conductivity copper. At the breech of the gun is a Vycor insulator and a gun header assembly. The header connects the gun electrodes through a parallel-plate transmission line to the capacitor bank cables. The header also served as a convenient place to connect an external crowbar switch (described in appendix B) during some of the experiments.

A short-duration puff of argon gas was admitted into the evacuated gun annulus through ports in the center electrode by a fast-acting mechanical gas valve. The duration of the gas puff was set experimentally at 100 microseconds. The mass per puff was controlled by the gas pressure in the valve plenum. An air-operated hammer provided the controlled blow to actuate the valve stem.

The dimensions and electrical characteristics of the four gun geometries investigated are given in table I. Geometries A and B used the same electrode radii (radius ratio of about 3), but the gas port location was changed. Geometry C employed gas ports at the breech, a glass baffle (to prevent gas reaching the breech to form a static secondary, i. e., a crowbar discharge), a low inductance breech configuration, and a larger radius ratio (7.5). Geometry D differed from geometry C only in its radius ratio (15) and shorter barrel. This design caused the gun current to be near zero when the plasma sheet was at the muzzle. In all experiments (except when geometry A was so operated that crowbar occurred at time of maximum current), a corona inhibitor ring covered a corner protruding in the breech. This delayed the time of crowbar.

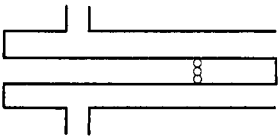
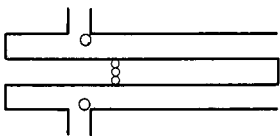
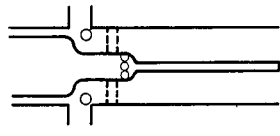
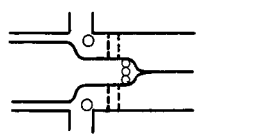
Instrumentation

Bank charging voltage was measured with calibrated voltmeters mounted on the bank control console. Gun exhaust energy was measured as the temperature rise of a calorimeter cup located 30 centimeters downstream of the gun. The temperature rise was recorded on a millivolt strip-chart recorder. The calorimeter cup (15 cm diam.) was constructed to reduce ablation errors and to absorb the beam energy efficiently.

Probes for the measurement of azimuthal magnetic field were inserted into the gun annulus, 11.5 centimeters apart, staggered along the gun axis (four in geometries A, B, and C and two in geometry D), and immersed in the annulus about 0.3 centimeter so as not to affect the plasma sheet. Time of flight of the magnetic front between two adjacent probe stations determined the front velocity. The magnetic probes had four turn coils, solenoidally wound about a 0.050-inch-diameter coil form and encased in a Vycor protector tube. The signals were transmitted via coaxial cables, terminated, passively inte-

TABLE I. - GUN GEOMETRIES AND CHARACTERISTICS

[Radius of gun center electrode, r_i ; radius of gun outer electrode, r_o ; effective gun length, ℓ ; gun length from initial discharge location to crowbar discharge location, ℓ_D ; parasitic resistance, R_p ; crowbar resistance, R_C ; parasitic inductance, L_p ; crowbar inductance, L_C ; gun inductance from crowbar discharge location to initial discharge location, L_D .]

Gun	Schematic	Gun dimensions, cm				Electrical characteristics					Nondimensional parameters				
		r_i	r_o	ℓ	ℓ_D	R_p , ohm	R_C , ohm	L_p , H	L_C , H	L_D , H	\mathcal{R}_p	\mathcal{R}_C	\mathcal{L}_p	\mathcal{L}_C	\mathcal{L}_D
A		1.6	4.75	30	18	3.8×10^{-3}	0	26×10^{-9}	1.0×10^{-9}	53×10^{-9}	0.0517	0	0.398	0.0153	0.81
							3.5×10^{-3}	14×10^{-9}	39×10^{-9}	65×10^{-9}	0.0517	0.047	0.212	0.575	0.985
B		1.6	4.75	46	2	3.8×10^{-3}	0	26×10^{-9}	1.0×10^{-9}	17×10^{-9}	0.0414	0	0.257	0.01	0.17
C		0.64	4.75	46	2	3.8×10^{-3}	-----	14×10^{-9}	-----	9×10^{-9}	0.0307	-----	0.0757	-----	0.0486
D		0.32	4.75	20	2	3.8×10^{-3}	-----	14×10^{-9}	-----	9×10^{-9}	0.0402	-----	0.129	-----	0.083

grated ($10\ \mu\text{sec}$ time constant), and recorded on an oscilloscope. The probes were calibrated by immersion in a known transient magnetic field with dynamics similar to that of the experiment.

Gun voltage, gun current, and the sequence of events were used to monitor the experiments.

EXPERIMENTAL PROCEDURE

The first step in the operating sequence for the experiments was to evacuate the gun and test section to the low (10^{-6} mm Hg) pressure region. A short duration puff of argon propellant was then injected between the electrodes. A controlled period of time was allowed for the gas to disperse between the electrodes and for the charged capacitor bank to be switched to the gun. After breakdown, the resulting plasma accelerated out of the gun and into the evacuated test section where it impinged on the calorimeter cup. In all reported data the center electrode was initially negative.

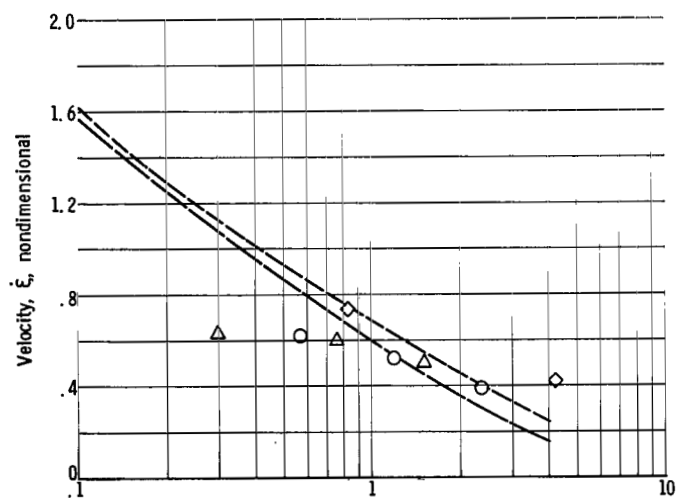
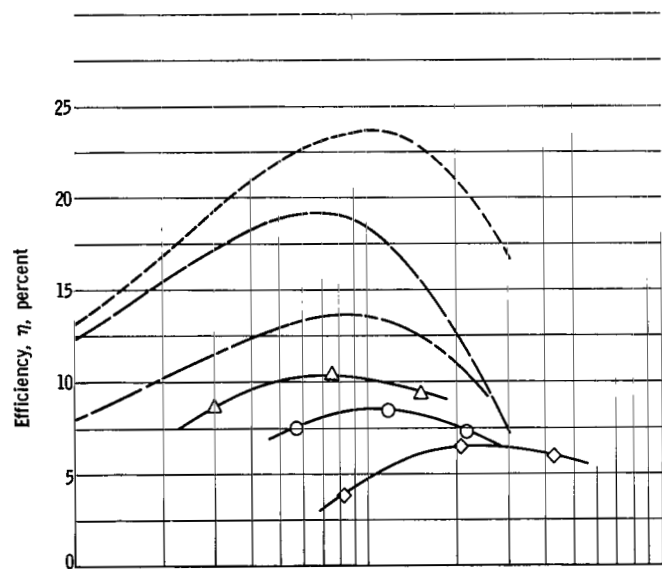
For each geometry, a series of shots was made to determine the optimum time delay between insertion of the gas puff and application of the bank voltage. This optimum delay time (with respect to kinetic efficiency) was used in the remainder of the shots with the same gun.

The following procedure was used to obtain each data point shown in figure 4:

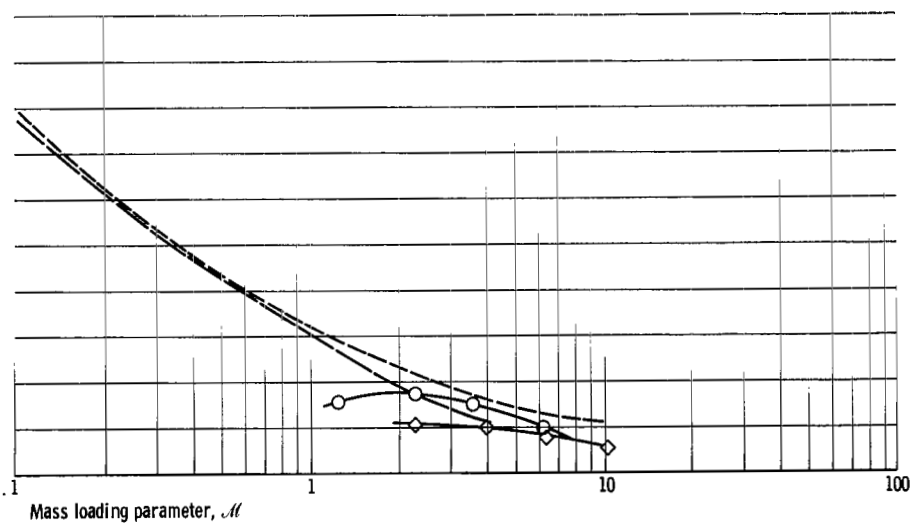
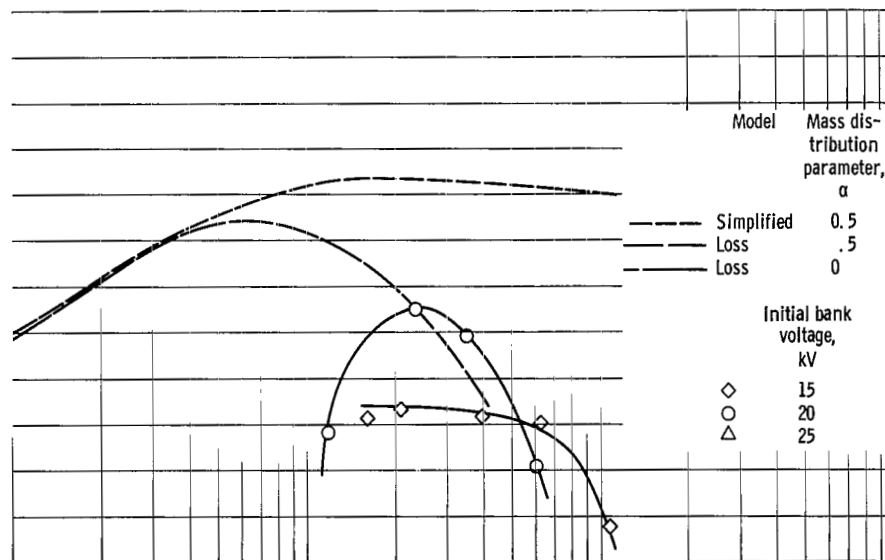
- (1) The mass per puff was calibrated just before the series of shots.
- (2) The gun was run 10 times to outgas and condition the electrodes.
- (3) All data were gathered simultaneously and synchronously for five identical shots.
- (4) The mass per puff was recalibrated.

The experimental data points on the figures are the average values of the five shots gathered.

The variation of efficiency and magnetic front velocity with mass over the practical operating range of the device was determined for three different bank voltages: 15, 20, and 25 kilovolts. The experimental gun efficiency was determined by dividing the energy received in the calorimeter cup by the difference between the energy originally stored in the bank and the switch loss energy (ref. 22). The calorimeter cup cannot differentiate between the thermal energy and the directed kinetic energy in the impinging exhaust. The exhaust has been assumed herein to be primarily directed kinetic energy. This assumption is justified, in part, by the fact that the theoretical thermal energy component is small when losses are included in the analysis (as discussed in the section Theoretical Performance).

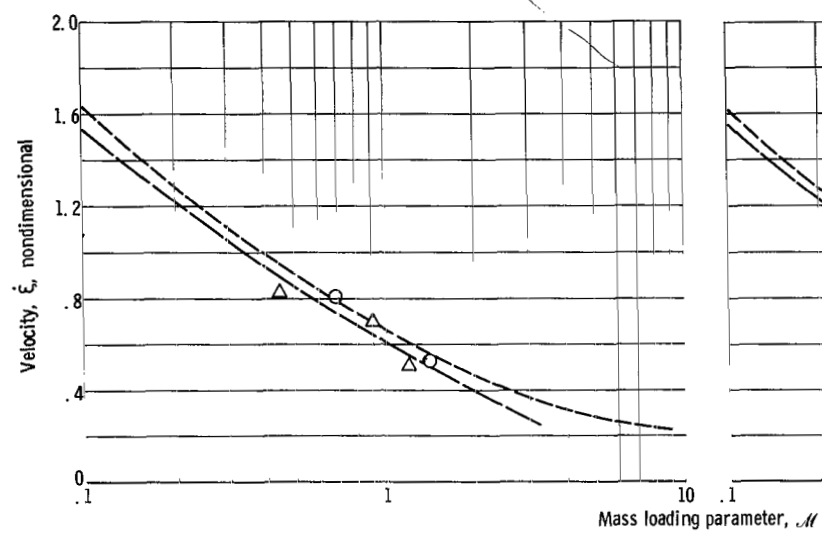
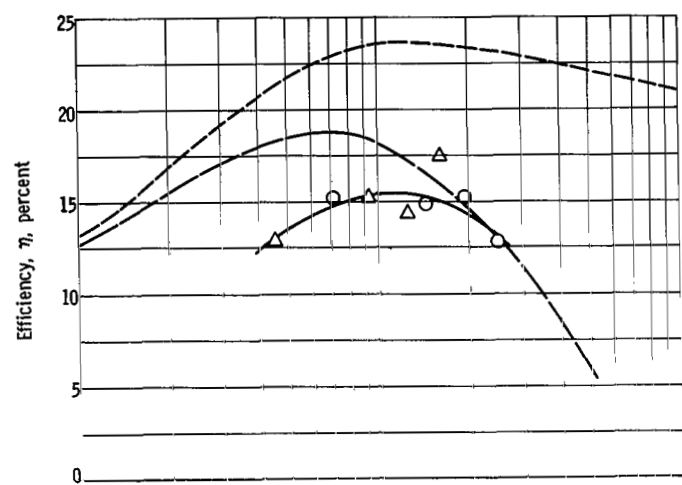


(a) Geometry A, not crowbarred.

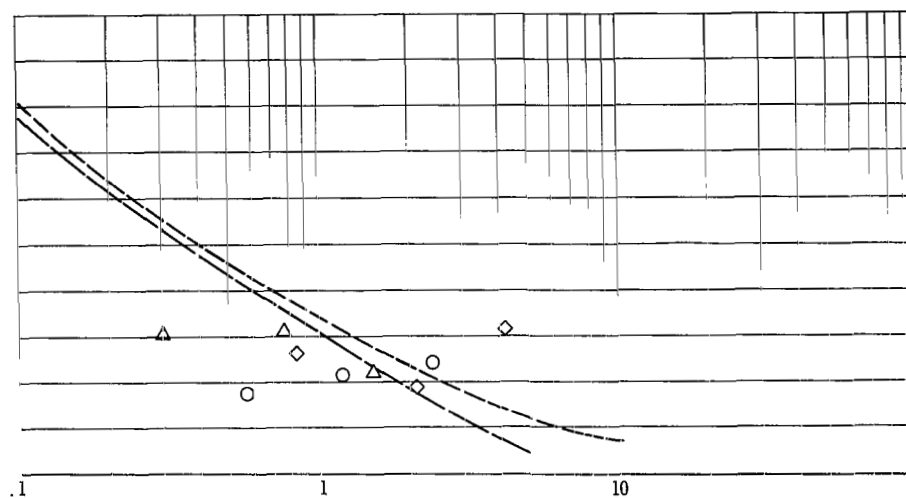
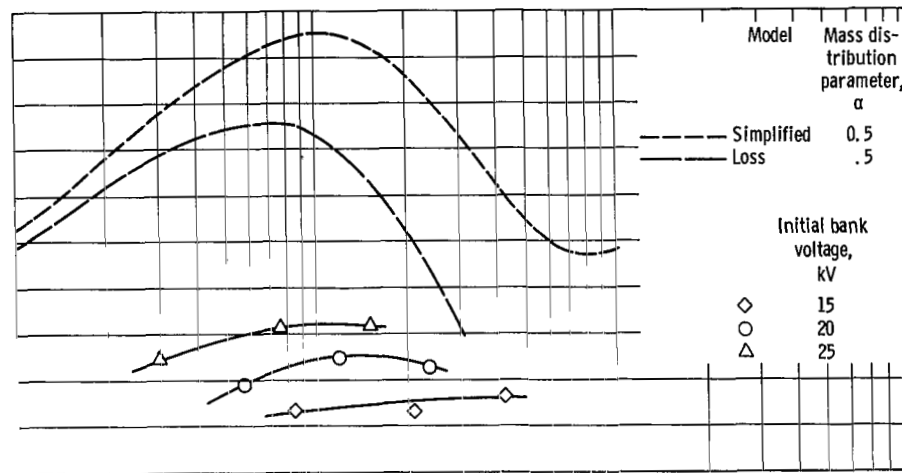


(b) Geometry A, early internal crowbar. Theoretical model crowbarred at maximum current.

Figure 4. - Theoretical and experimental performance of various plasma-gun geometries.

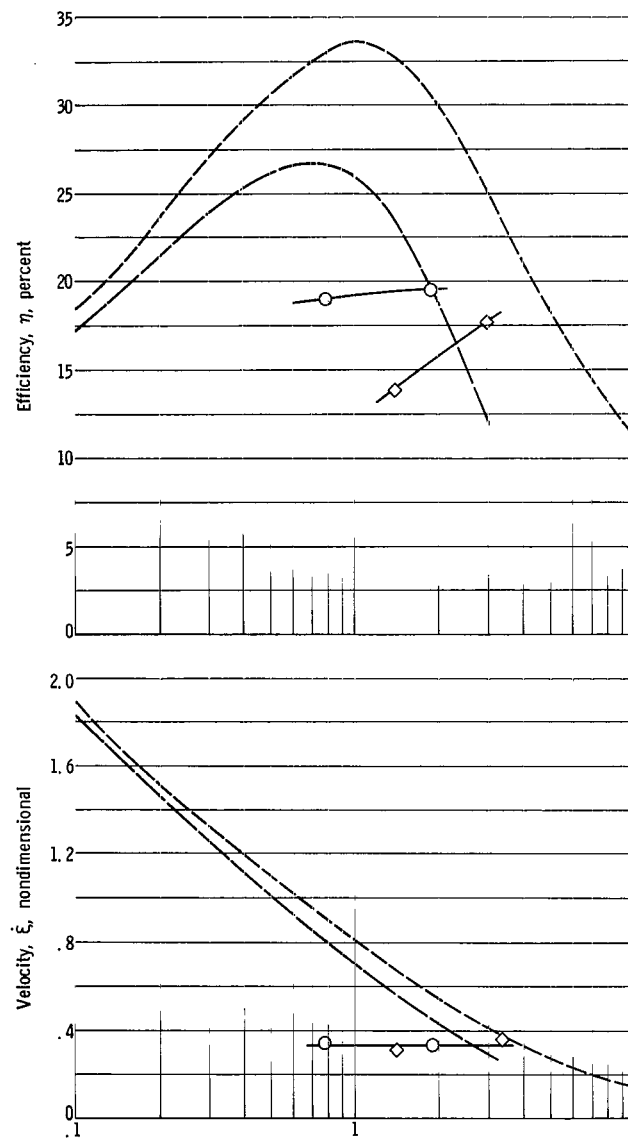


(c) Geometry A, delayed internal crowbar. Theoretical model crowbarred at maximum energy.

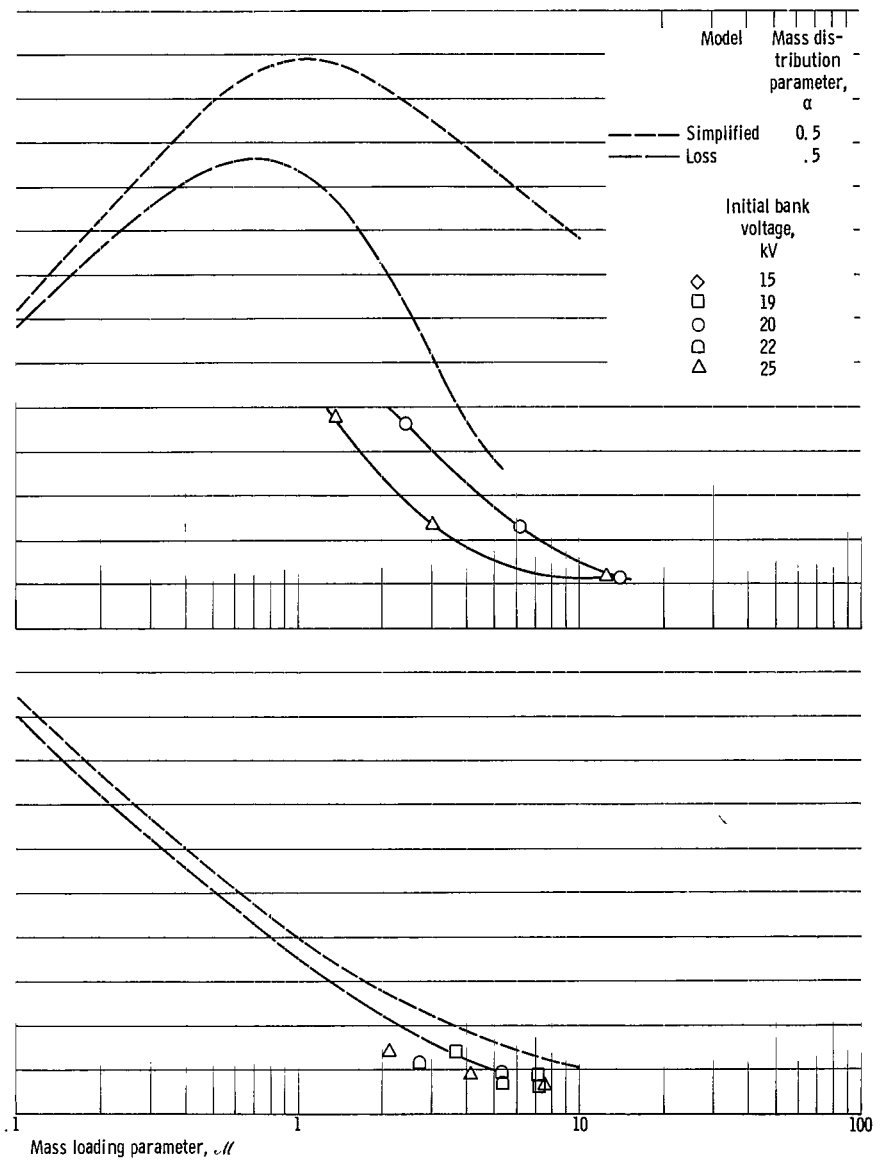


(d) Geometry A, externally crowbarred. Theoretical model crowbarred at maximum energy.

Figure 4. - Continued.

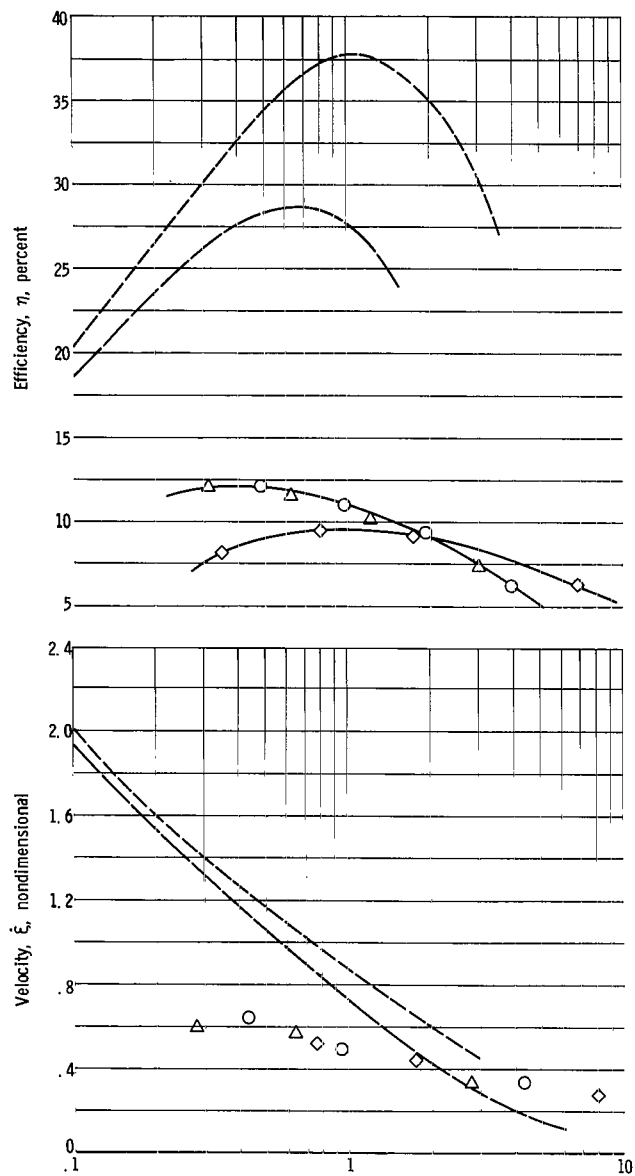


(e) Geometry B, noncrowbarred.

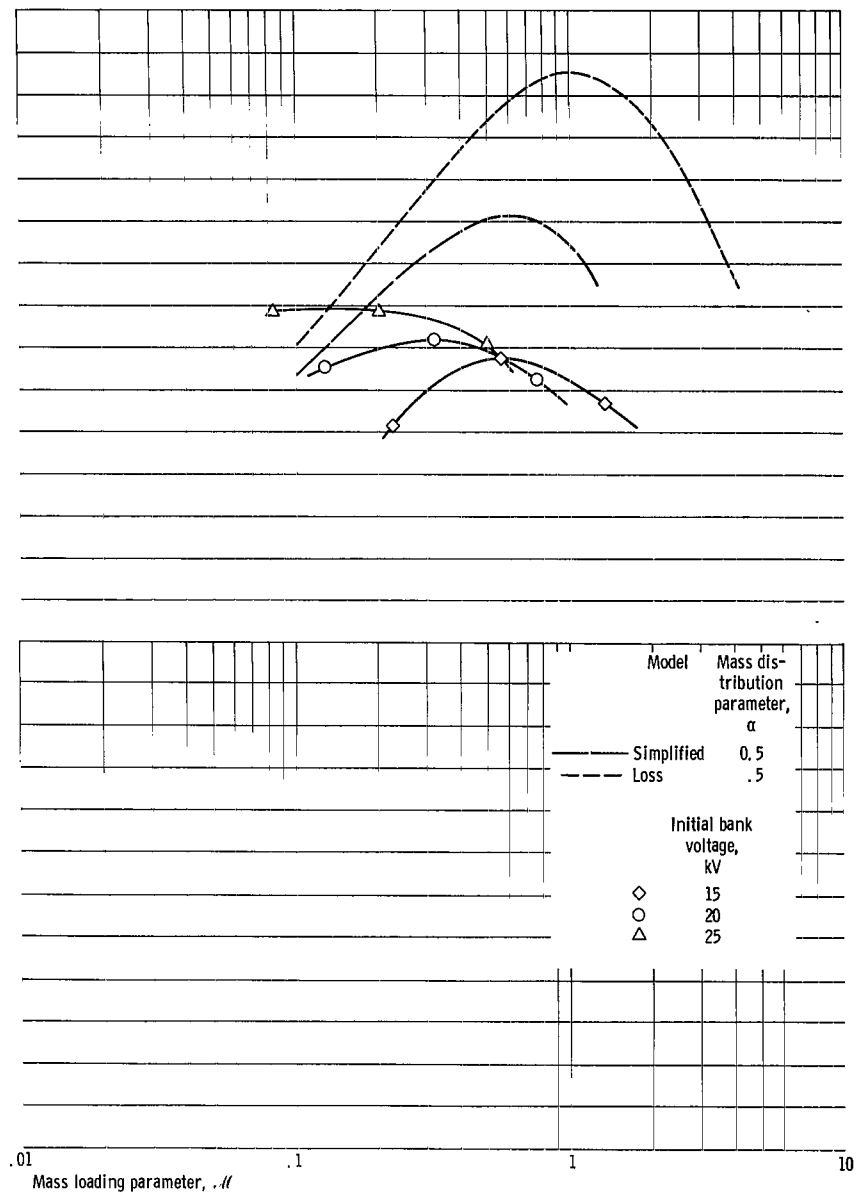


(f) Geometry B, delayed internal crowbar. Theoretical model crowbarred at maximum energy.

Figure 4. - Continued.



(g) Geometry C, not crowbarred.



(h) Geometry D, not crowbarred.

Figure 4. - Concluded.

COMPARISON OF THEORY WITH EXPERIMENT

The experimental and theoretical energy efficiencies and velocities determined for each geometry are presented as a function of the mass loading parameter \mathcal{M} in figure 4. Theoretical efficiencies are presented for both the simplified and loss models.

Neutral gas-pressure profiles in the gun as a function of time were measured prior to the experiment for a geometry similar to geometry A (without the glass baffle). From knowing the time delay for optimum experimental efficiency and the shape of the pressure profile at that time the mass distribution factor α was estimated to be approximately 1/2. Pressure profiles against time for the other geometries were not determined but an α of 1/2 was used for calculating all theoretical efficiencies.

The loss parameters evaluated for each geometry in determining the theoretical efficiency for the loss model are shown in table II. These parameters were mostly determined from the configuration in table I and the general or estimated values indicated in table II.

The experimental efficiency curves are plotted for a limited range of \mathcal{M} values. For low values of mass inserted in the gun annulus (low values of \mathcal{M}), the statistical breakdown delay time (time between voltage application and ignition) increases. Estimation of M_0 and α for the theoretical analysis therefore becomes difficult, and the data are not repeatable because of the nonuniform breakdown time. The experimental curves terminate when \mathcal{M} is reduced to the point where breakdown delay is longer than 10 microseconds. For large values of inserted mass, the discharge becomes diffuse. The curves

TABLE II. - LOSS PARAMETERS

[Thickness of current sheet, Δx , 0.01 m; effective ionization potential per ion, Φ_i , 1.12×10^{-17} J (70 eV); effective excitation potential per ion, Φ_e , 6.42×10^{-18} J (40 eV); fraction of ions in excited state, g , 1.0; charge number of ions, z , 2.0; mean lifetime of excited state, t_e , 2.5×10^{-8} sec.]

Geometry	Nondimensional parameters				
	Diffusion coefficient, δ	Effective potential, φ_1	Excitation loss parameter, φ_2	Convection cooling coefficient, Ω	Heat conduction parameter, \mathcal{J}
A	4.77	2.35×10^{-3}	3.06×10^{-2}	3.5	1.0×10^9
B	7.62	1.46×10^{-3}	2.41×10^{-2}	5.6	2.0×10^{10}
C	5.57	2.80×10^{-3}	6.1×10^{-2}	2.94	1.0×10^9
D	2.26	8.70×10^{-3}	1.45×10^{-1}	.949	8.0×10^6

terminate when the steepness of the magnetic fronts measured in the gun annulus becomes so small that estimating the sheet velocity becomes difficult.

The maximum theoretical kinetic energy efficiency for the simplified model (ref. 1), for α equal to $1/2$, is 40 percent when \mathcal{M} equals 1.2 and \mathcal{L}_{tot} equals 0.092. Even though geometries C and D are most nearly like this model, a survey at this \mathcal{M} value showed that none of the geometries had an efficiency greater than 22.2 percent.

Other practical factors not included in the analysis also have effects on the maximum kinetic energy efficiency. For example, for a gas propellant, the simplified model optimum solutions suggest insertion of the gas as a slug at the breech. However, very poor efficiencies were noted when this mass distribution was attempted experimentally (by a very short delay between injection and bank voltage application). Magnetic probes indicated that "spoking instabilities," which prevent the efficient sweep-up of gas, exist for these cases. These instabilities decrease the efficiency well below the theoretical value for α near 1, while even the theoretical efficiency is poor when α is near zero. That optimum experimental efficiency occurs for intermediate values of α (e.g., $\alpha = 1/2$ for geometry A, internally crowbarred) is therefore understandable. The experimental efficiency for most geometries was significantly affected by initial bank voltage. This effect did not agree with the theoretical analysis, which predicted a much smaller voltage effect in the opposite direction. The small effect of bank voltage permitted the use of one bank voltage, 25 kilovolts, to determine the loss parameters of table II and the theoretical curves of figure 4.

The experimental and theoretical efficiency and velocity are shown as a function of the mass loading parameter \mathcal{M} for noncrowbarred geometry A in figure 4(a) (p. 15). A Vycor baffle was placed just upstream of the gas ports in the gun annulus for this case to prevent gas from drifting toward the breech and eventually providing conditions for developing a second static crowbar discharge. The mass distribution for this mode of operation was not measured. Theoretical loss model efficiency curves are shown for α equal to $1/2$ and 0 to emphasize the need for accurate knowledge of mass distribution before attempting precision comparisons of theory with experiment.

Figure 4(b) (p. 15) is for the same geometry operated without the glass baffle so that it crowbarred internally. In this experiment, the breech outer electrode connection had a relatively sharp radius edge on which the crowbar discharge could seat. The gun crowbarred at close to maximum current time. The 20 kilovolt experimental data straddle the loss model curve for \mathcal{M} greater than 2.0 to within 2 percent. The 15 kilovolt data are in poorer agreement except near \mathcal{M} equal to 3.0.

The same geometry, operated crowbarred internally without the glass baffle but with a ring to inhibit crowbar breakdown on the sharp edge at the breech, provided the data shown in figure 4(c) (p. 16). The presence of the ring delayed the time of crowbar relative to the previously mentioned case (closer to the case for crowbar at maximum

energy). The experimental efficiencies are within 3 percent of the loss model predictions for \mathcal{M} greater than 0.7. The efficiencies increased for the delayed crowbarring as compared with the other crowbar case and peaked at values of \mathcal{M} closer to 1. Both these quantitative findings appear to be in agreement with the simplified and loss analyses.

An external crowbar switch was connected across the header terminals of geometry A. Figure 4(d) (p. 16) shows the data for external crowbar at maximum current time (experimentally determined as optimum time of crowbar). In order that the crowbar switch efficiently trap the energy in the gun, the crowbar switch impedance should be about one-tenth the bank system impedance. A crowbar switch with impedance lower than an already very low impedance bank system was physically impractical. External crowbar was nevertheless attempted, because independent control of crowbar switching could be achieved.

A glass baffle was placed just upstream of the gas ports to prevent internal crowbarring at the breech for the experiment. The theoretical loss-model efficiency curve is similar to the corresponding noncrowbarred curve of figure 4(a), because the external crowbar impedance is relatively large. The experimental efficiency data for the external crowbar (fig. 4(d)) are generally a few percent lower than the corresponding noncrowbarred data (fig. 4(a)). This difference is probably due to the external crowbar switch losses. The comments concerning mass distribution (discussed on p. 20) for figure 4(a) apply to figure 4(d) also.

Figure 4(e) (p. 17) shows the data for geometry B operated noncrowbarred. A glass baffle was inserted upstream of the gas ports to prevent gas from drifting toward the breech and eventually to provide conditions for developing a crowbar discharge. Limited experimental data were available.

In the experimental curves of geometry B operated internally crowbarred (fig. 4(f), p. 17), the voltage again causes some shifts in the efficiency curves. The crowbar occurred later than at maximum current time and is compared with theoretical values for crowbar at maximum energy time. This geometry operated at very low injected masses, and breakdown delay times beyond 10 microseconds made data gathering impractical for \mathcal{M} approximately 1.0 or less.

The experimental data for geometries C and D, which have large radius ratios are shown in figures 4(g) and (h) (p. 18), respectively. Noncrowbarred operation was observed for both with the glass baffle (shown by dashed lines in table I, p. 13) in place. Spectra indicated that both geometries had substantial quantities of electrode material in the exhaust. This erosion could affect the \mathcal{M} chosen, especially in geometry D. Typical plasma spectra are discussed in appendix C. No experimental velocity data were recorded for geometry D since erosion seriously affected the data.

Geometry D yielded substantially higher efficiencies than geometry C even though peak theoretical efficiencies predicted by the loss are almost the same (27.8 and 28.6

percent, respectively). Geometry D had a shorter barrel length to reduce wall losses, and the radius ratio was doubled compared with geometry C to show the effect of L' on performance while maintaining almost the same $L'l$ product.

For geometry D, the maximum experimental efficiency is 22.2 percent, which is about 60 percent of the peak value predicted by the simplified model and about 75 percent of the peak value for the theoretical loss model. For 15 kilovolts, if M were increased to account for eroded electrode material in the exhaust, these experimental peaks might be near the predicted optimum values of M .

The uncertainty in determining experimental velocity when probe traces are difficult to interpret is probably the reason for generally lower than predicted velocities especially for M greater than 1.0. In all but one case (geometry A, delayed internal crowbar), the velocities measured are significantly lower than the predicted values for M smaller than 1.0. These unexpectedly low velocities are probably the result of a compounding of effects due to uncertainty in measuring velocity and M .

CONCLUDING REMARKS

Experimental calorimetric exhaust efficiencies and magnetic front velocities were compared with the prediction of a theory based on the snowplow model. Four gun geometries were studied for a range of initial masses of argon propellant and initial voltages. The guns were operated in several modes: noncrowbarred, crowbarred internally at the time of maximum current, crowbarred internally at a later, more nearly optimum, time, and crowbarred externally at maximum current time.

Comparisons of the experimental results with the predictions of the theory indicate general qualitative agreement of efficiency and sheet velocity. The predicted kinetic energy efficiencies and velocities, however, are consistently higher than measured values. These discrepancies might be attributed to an incorrect assumption for the mass distribution because no measurements of distribution were made for this geometry.

The predictions regarding the effect of crowbar were also in qualitative agreement with the experimental results. For one gun geometry, however, the peak efficiency for the crowbarred mode was larger than that of the noncrowbarred mode, contrary to the predictions of the theory. However, the presence of the glass baffle in the gun that operated in the noncrowbarred mode might have significantly changed the shape of the mass distribution and thus obscured the comparison.

The theoretical model presented is useful for the determination of relevant parameters and is adequate to predict qualitative trends. More accurate predictions probably require a more sophisticated model.

Because theory suggests the use of a sharply decreasing (slug) mass loading distribution, future experimental efforts should be directed toward producing and measuring such distributions while attempting to suppress the instabilities that seem to be associated with these distributions.

Lewis Research Center,
National Aeronautics and Space Administration,
Cleveland, Ohio, March 18, 1966.

APPENDIX A

SYMBOLS

C	capacitance, F	m_e	electron mass, 9.107×10^{-31} kg
e	electronic charge, 1.602×10^{-19} , C	m_i	ion mass, kg
f	nondimensional mass distribution function, $M(x)/M_0$	P	nondimensional thermal ionization factor
g	fraction of ions in excited state	Q	charge in capacitor, C
I	current, A	Q_0	initial charge in capacitor, C
\mathcal{I}	nondimensional gun current, $I_G / (CV_0 / \sqrt{L'\ell C})$	R	resistance, ohm
\mathcal{J}	nondimensional heat conduction parameter (eq. (6))	\mathcal{R}	nondimensional resistance, $(C/L'\ell)^{1/2} R$
K	coefficient of thermal conductivity, $J/(\text{sec})(m)(^\circ K)$	r_i	radius of gun center electrode, m
k	Boltzmann constant, 1.38×10^{-23} , $J/^\circ K$	r_o	radius of gun outer electrode, m
L	inductance, H	S	area, sq m
L_D	gun inductance from crowbar discharge location to initial discharge location, $L_D = L'\ell_D$, H	T	mean plasma temperature, $^\circ K$
L'	inductance per unit length, $2 \times 10^{-7} \ln(r_o/r_i)$, H/m	t	time, sec
\mathcal{L}	nondimensional inductance, $(1/L'\ell)L$	t_e	mean lifetime of excited state, sec
ℓ	effective gun length, m	V	capacitor voltage at time t, V
M	mass swept up by moving discharge, $M = M(x)$, kg	V_0	initial voltage supplied to the capacitor, V
M_0	total injected mass per shot, kg	x	distance of current sheet from initial discharge position, m
\mathcal{M}	nondimensional mass loading parameter, $(2\ell/L'Q_0^2)M_0$	Δx	thickness of current sheet, m
		z	charge number of ions
		α	nondimensional mass distribution parameter (eq. (7))
		β	nondimensional temperature, $\frac{2k}{m_i} \left(\frac{L'C}{\ell} \right) T$

Γ	ion diffusion current, particles/sec
γ	nondimensional charge, $Q_0^{-1} Q$
δ	nondimensional diffusion coefficient, $[1/2(r_0 - r_i)]\ell$
ϵ_0	permittivity of free space, 8.85×10^{-12} F/m
η	nondimensional kinetic efficiency, $1/2 \mathcal{M} f \xi^2$
Λ	ratio of Debye length to Rutherford impact parameter
ξ	nondimensional length, $\ell^{-1} x$
τ	nondimensional time, $(L'C\ell)^{-1/2} t$
Φ_e	effective excitation potential per ion, J
Φ_i	effective ionization potential per ion, J
Φ_1	combined effective potential, $\Phi_1 = \Phi_i + g\Phi_e$, J
Φ_2	excitation loss rate parameter, $\Phi_2 = g\Phi_e/t_e$, J/sec
φ_1	nondimensional effective potential, $\varphi_1 = \Phi_1/(m_i\ell/L'C)$
φ_2	nondimensional excitation loss parameter, $\varphi_2 = \Phi_2 \sqrt{L'\ell C}/(m_i\ell/L'C)$

Ω nondimensional convection cooling
coefficient, $3/2 (m_i\ell/L'C)/eV_0$

Subscripts:

B	bank
C	crowbar
D	from crowbar discharge location to initial discharge location
G	gun
P	plasma
p	parasitic
tot	total

Superscripts:

'	first derivative with respect to non- dimensional time
''	second derivative with respect to nondimensional time
'	first derivative with respect to non- dimensional distance

APPENDIX B

EXTERNAL CROWBAR SYSTEM

by Fred F. Terdan

"Closing" an ignitron switch when the voltage across it is only 100 volts or less introduces serious variation in closing time (jitter). This situation occurs when an ignitron is used as an external crowbar switch for a coaxial plasma gun. The gun should be crowbarred at the time of maximum current. This maximum current corresponds to near zero gun voltage, and at that instant, an ignitron crowbar switch will have excessive jitter.

The desired approach was to use ignitron circuitry, but conventional ignitron circuitry will not switch controllably at zero voltage. An ignitron biasing technique was developed, and this technique allowed controllable switching to occur at zero voltage.

The external crowbar systems described in references 23 to 25 were not practical for this experiment when studied in terms of the characteristics of the existing capacitor bank. The biased ignitron circuitry developed for this experiment was suitable in all characteristics with the exception that it was inefficient because the switch impedance was higher than the bank impedance.

The schematic diagram for the external crowbar system is shown in figure 5. The complete unit consists of the crowbar switch (three pairs of parallel GL-7703 ignitrons), a trigger amplifier (incorporating three stages of amplification utilizing a 2D21 thyratron, a 5C22 thyratron, and a GL-7703 ignitron), a control system, and the necessary power supplies. Three back-to-back pairs of parallel ignitrons were chosen to provide necessary voltage holdoff capability, current carrying capacity, low inductance, and low voltage switching ability. Capacitors of 1 microfarad placed across each set of three ignitrons were precharged to opposite polarities. Charging is accomplished by a remotely operated power supply just prior to the use of the crowbar switch. The charged capacitors provided some of the energy lost in making the crowbar switch conduct. These capacitors and a water system that controlled ignitron temperature were necessary to reduce the switch jitter to less than 0.2 microsecond. Figure 6 shows a view of the crowbar ignitrons, the capacitors in the crowbar system, and the gun header. The total inductance of the crowbar switch is 39 nanohenries, and the static crowbar switch resistance is approximately 3.5×10^{-3} ohm. This assembly holds off 25 kilovolts and can be activated (with 0.2 μ sec jitter time) for header voltages above a few hundred volts.

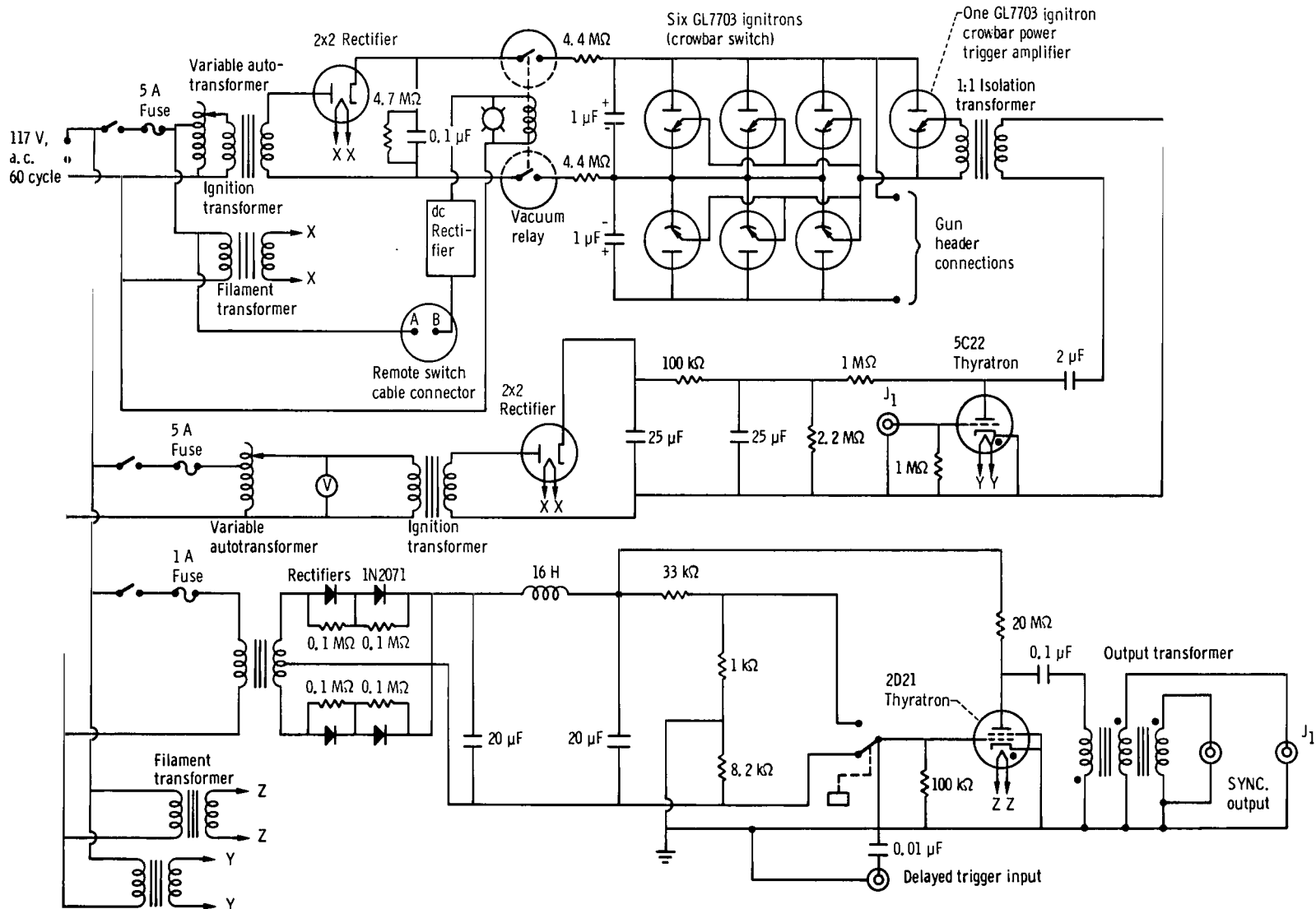


Figure 5. - Schematic diagram of external crowbar system.

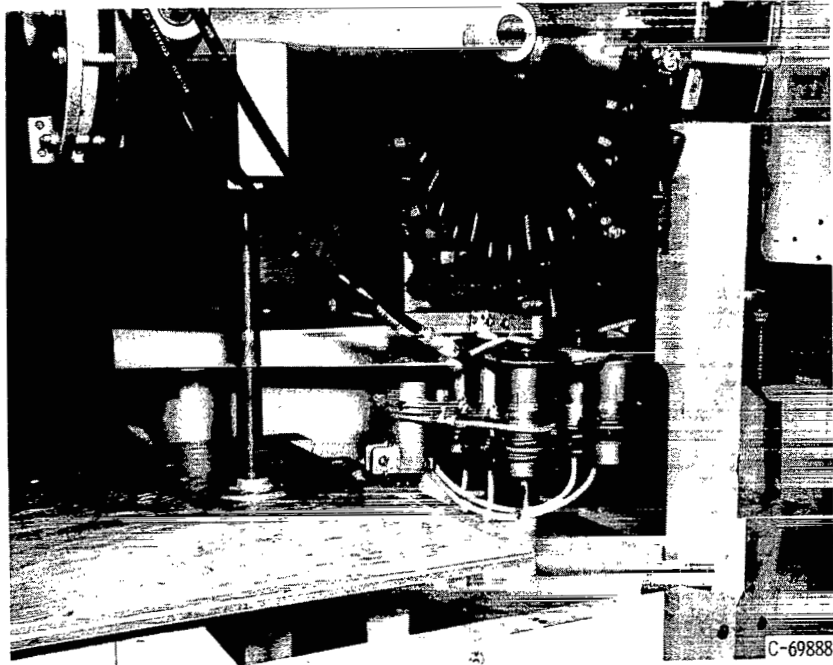


Figure 6. - External crowbar system.

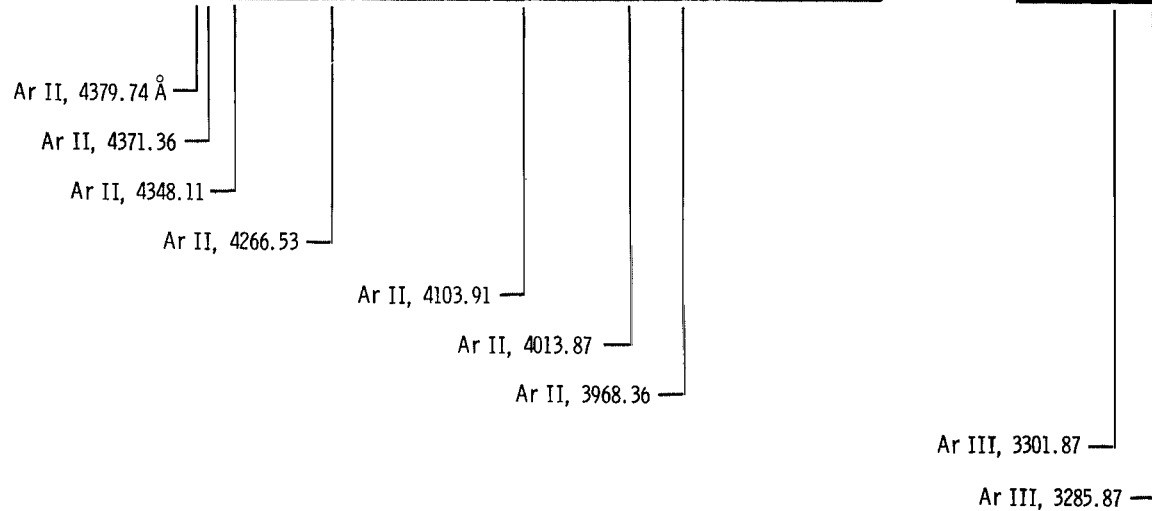
APPENDIX C

SPECTROSCOPIC OBSERVATIONS

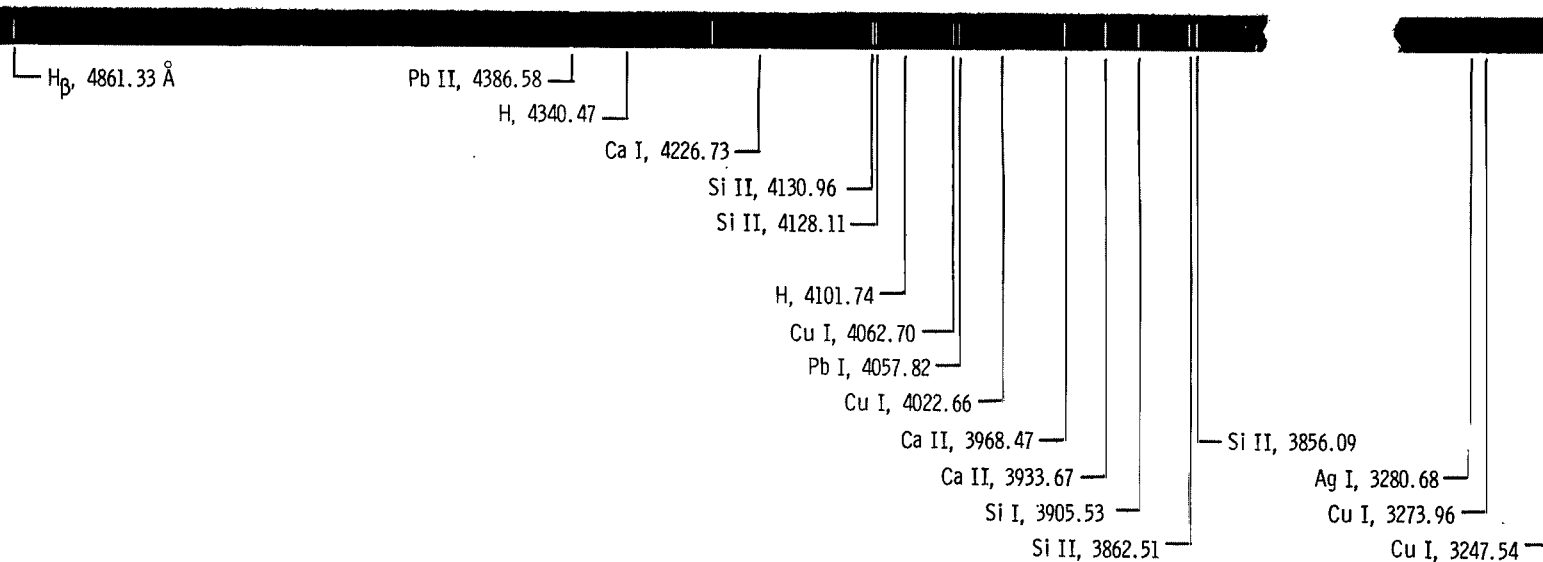
The discharges of two different gun geometries were examined with a $1\frac{1}{2}$ -meter grating spectrograph. The first-order dispersion of the instrument was 20 \AA per millimeter. Since the discharge is of such short duration, a series of 25 shots was superimposed to expose the spectrographic film sufficiently. Reflected light did not have sufficient intensity to record on the film. The spectra recorded are due to the time-integrated light from the discharges that were in the viewing area. Film limitations placed the lower viewing limit at 2400 \AA .

The discharge in the annulus of geometry A was viewed radially (i. e. , normal to the gun axis) through a fused quartz window in the outer barrel. Figure 7(a) shows the spectrograph obtained with geometry A operated internally crowbarred at 20 kilovolts and with argon propellant. (These spectra were identified and interpreted by Henry J. Hettel of Lewis.) The window was located 41.5 centimeters from the breech end of the gun (6.5 cm upstream of the gun muzzle). Argon II and argon III lines are noted and the discharge is relatively free from contaminants. From these qualitative measurements, the effective ionization potential per ion for argon was estimated to be 30 electron volts. This value was used to calculate the nondimensional effective potential ϕ_1 listed in table II (p. 19). The effective excitation potential was estimated as 40 electron volts per ion and was used to calculate the nondimensional excitation loss parameter ϕ_2 , also listed in table II.

In contrast, the spectrum for a modified geometry D gun (radius ratio, 7.5 and without the glass baffle), using argon is shown in figure 7(b). The device was also operated internally crowbarred at 20 kilovolts. The spectrograph viewed the exhaust in a part of the gun annulus as it left the gun muzzle. The line of sight was at a 45° angle to the gun axis, looking into the gun muzzle through a heat-resistant glass drift tube. Electrode material (copper and solder) and glass dominate the spectrum and no argon propellant lines are observed. The glass spectrum probably is caused by the excitation of the heat-resistant glass tube as the plasma exhaust collides with the tube wall downstream of the gun muzzle. The presence of copper lines and the lack of argon lines of any appreciable intensity indicates that the device is probably operating on metal-derived plasma or some combination thereof.



(a) Radial view near muzzle annulus of geometry A.



(b) Modified geometry D viewed at 45° angle to muzzle annulus.

Figure 7. - Section of visible spectrum of coaxial plasma-gun discharge.

REFERENCES

1. Michels, C. J.; Heighway, J. E.; and Johansen, A. E.: Analytical and Experimental Performance of Capacitor Powered Coaxial Plasma Guns. Paper No. 65-340, AIAA, July 1965.
2. Dattner, A.: Acceleration of Plasma. Vol. 2 of the Proceedings of the Fourth International Conference On Ionization Phenomena in Gases, N. Robert Nilsson, ed., North-Holland Pub. Co., 1960, pp. IVE 1151-1155.
3. Lovberg, R. H.; Hayworth, B. R.; and Gooding, T. J.: The Use of a Coaxial Gun for Plasma Propulsion. Final Rep. No. AE62-0678, General Dynamics/Astronautics, May 1962.
4. Vargo, Donald J.: Electromagnetic Acceleration of a Variable-Mass Plasma. NASA TN D-2164, 1964.
5. Hart, Philip J.: Modified Snowplow Model for Coaxial Plasma Accelerators. J. Appl. Phys., vol. 35, no. 12, Dec. 1964, pp. 3425-3431.
6. Schock, A.: Electromagnetic Acceleration of Plasma for Space Propulsion. Planetary Space Sci., vol. 4, 1961, pp. 133-144.
7. Mostov, Philip M.; Neuringer, Joseph L.; and Rigney, Donald S.: Electromagnetic Acceleration of a Plasma Slug. Phys. Fluids, vol. 4, no. 9, Sept. 1961, pp. 1097-1104.
8. Artsimovich, L. A.; Luk'ianov, S. Iu.; Podgornyi, I. M.; and Chuvatin, S. A.: Electrodynamic Acceleration of Plasma Bunches. Soviet Phys.-JETP, vol. 6, no. 1, Jan. 1958, pp. 1-5.
9. Linhart, J. G.: A Simplified Analysis of the Dynamics of Plasma Guns. Nucl. Fusion, vol. 1, no. 2, Mar. 1961, pp. 78-81.
10. Kemp, Nelson H.; and Petschek, Harry E.: Theory of the Flow in the Magnetic Annular Shock Tube. Res. Rep. No. 60, AVCO Everett Res. Lab., July 1959.
11. Chang, C. T.: Shock Wave Phenomena in Coaxial Plasma Guns. Phys. Fluids, vol. 4, no. 9, Sept. 1961, pp. 1085-1096.
12. Gorowitz, B.; Gloersen, P.; and Rowe, J. H.: Performance Study of a Repetitively Pulsed Two-Stage Plasma Propulsion Engine. Final Rep., General Electric Co. (NASA CR-55248), Nov. 1963.
13. Kash, Sidney W.: Efficiency Considerations in Electrical Propulsion. Plasma Acceleration: Fourth Symposium on Magnetohydrodynamics, Sidney W. Kash, ed., Stanford University Press, 1960, pp. 79-93.

14. Mather, J. W. : High-Density Plasma Focus. Semiannual status report of the LASL Controlled Thermonuclear Research Program for the Period Ending April 20, 1964. Rep. No. LAMS 3085, Los Alamos Scientific Laboratory, May 1964, pp. 22-25.
15. Michels, Charles J. ; and Ramins, Peter: Performance of a Coaxial Plasma Gun with Various Propellants. Phys. Fluids, vol. 7, no. 11, pt. 2, Nov. 1964, pp. S71-S74.
16. Michels, Charles J. : Some Transient Electrical Characteristics of the Exhaust of a Self-Crowbarred Coaxial Plasma Gun. NASA TN D-2571, 1965.
17. Gooding, Terence J. ; Hayworth, Bruce R. ; Larson, Alan V. ; and Ashby, David E. T. F. : Development of a Coaxial Plasma Gun for Space Propulsion. Rep. No. GDA-DBE-64-051, General Dynamics/Astronautics (NASA CR-54149), June 1964.
18. Eubank, H. P. ; and Wilkerson, T. D. : Ion Energy Analyzer for Plasma Measurements. Rev. Sci. Instr., vol. 34, no. 1, Jan. 1963, pp. 12-18.
19. Henins, I. ; and Marshall, John: Hydromagnetic Plasma Gun Program. Semiannual Status Report of the LASL Controlled Thermonuclear Research Program for the Period Ending April 20, 1964. Rep. No. LAMS-3085, Los Alamos Scientific Laboratory, May 1964, pp. 56-71.
20. Gooding, Terence J. ; Larson, Alan V. ; Hayworth, Bruce R. ; and Ashby, David E. T. F. : Development of a Coaxial Plasma Gun for Space Propulsion. Final Rep. No. GDA-DBE-64-052-4, General Dynamics/Convair (NASA CR-54245), Apr. 1965.
21. Chapman, S. : The Viscosity and Thermal Conductivity of a Completely Ionized Gas. Astro Phys. J., vol. 120, July 1954, pp. 151-155.
22. Michels, Charles J. ; and Terdan, Fred F. : Characteristics of a 5-Kilojoule, Ignitron-Switched, Fast-Capacitor Bank. NASA TN D-2808, 1965.
23. Mather, J. W. : Investigation of the High-Energy Acceleration Mode in the Coaxial Gun. Phys. Fluids, vol. 7, no. 11, pt. 2, Nov. 1964, pp. S28-S34.
24. Hagerman, D. C. ; and Osher, J. E. : Two High Velocity Plasma Guns. Rev. Sci. Instr., vol. 34, no. 1, Jan. 1963, pp. 56-60.
25. Mather, J. W. ; and Williams, A. H. : Some Properties of a Graded Vacuum Spark Gap. Rev. Sci. Instr., vol. 31, no. 3, Mar. 1960, pp. 297-307.

"The aeronautical and space activities of the United States shall be conducted so as to contribute . . . to the expansion of human knowledge of phenomena in the atmosphere and space. The Administration shall provide for the widest practicable and appropriate dissemination of information concerning its activities and the results thereof."

—NATIONAL AERONAUTICS AND SPACE ACT OF 1958

NASA SCIENTIFIC AND TECHNICAL PUBLICATIONS

TECHNICAL REPORTS: Scientific and technical information considered important, complete, and a lasting contribution to existing knowledge.

TECHNICAL NOTES: Information less broad in scope but nevertheless of importance as a contribution to existing knowledge.

TECHNICAL MEMORANDUMS: Information receiving limited distribution because of preliminary data, security classification, or other reasons.

CONTRACTOR REPORTS: Technical information generated in connection with a NASA contract or grant and released under NASA auspices.

TECHNICAL TRANSLATIONS: Information published in a foreign language considered to merit NASA distribution in English.

TECHNICAL REPRINTS: Information derived from NASA activities and initially published in the form of journal articles.

SPECIAL PUBLICATIONS: Information derived from or of value to NASA activities but not necessarily reporting the results of individual NASA-programmed scientific efforts. Publications include conference proceedings, monographs, data compilations, handbooks, sourcebooks, and special bibliographies.

Details on the availability of these publications may be obtained from:

SCIENTIFIC AND TECHNICAL INFORMATION DIVISION
NATIONAL AERONAUTICS AND SPACE ADMINISTRATION
Washington, D.C. 20546